

27. Kessel, R. L. *et al.* Evidence of high-latitude reconnection during northward IMF: Hawkeye observations. *Geophys. Res. Lett.* **23**, 583–586 (1996).
28. Miura, A. & Pritchett, P. L. Nonlocal stability analysis of the MHD Kelvin-Helmholtz instability in a compressible plasma. *J. Geophys. Res.* **87**, 7431–7444 (1982).
29. Report of the NASA Science and Technology Definition Team for the Magnetospheric Multiscale (MMS) Mission (NASA/TM-2000-209883, Goddard Space Flight Center, Greenbelt, MD, 1999).

Supplementary Information accompanies the paper on www.nature.com/nature.

Acknowledgements We are indebted to the Cluster team for the design and successful operation of the Cluster II mission. Part of this work was done while H.H. visited UC Berkeley.

Competing interests statement The authors declare that they have no competing financial interests.

Correspondence and requests for materials should be addressed to H.H. (hiroschi.hasegawa@dartmouth.edu).

Room-temperature ferroelectricity in strained SrTiO₃

J. H. Haeni¹, P. Irvin², W. Chang³, R. Uecker⁴, P. Reiche⁴, Y. L. Li¹, S. Choudhury¹, W. Tian⁵, M. E. Hawley⁶, B. Craigo⁷, A. K. Tagantsev⁸, X. Q. Pan⁵, S. K. Streiffer⁹, L. Q. Chen¹, S. W. Kirchoefer³, J. Levy² & D. G. Schlom¹

¹Department of Materials Science and Engineering, Penn State University, University Park, Pennsylvania 16802-5005, USA

²Department of Physics and Astronomy, University of Pittsburgh, Pittsburgh, Pennsylvania 15260, USA

³Naval Research Laboratory, 4555 Overlook Avenue S.W., Washington DC 20375, USA

⁴Institute of Crystal Growth, Max-Born-Straße 2, D-12489 Berlin, Germany

⁵Department of Materials Science & Engineering, University of Michigan, Ann Arbor, Michigan 48109-2136, USA

⁶Materials Science and Technology Division (MST-8), Los Alamos National Laboratory, Los Alamos, New Mexico 87545, USA

⁷Motorola Labs, 2100 East Elliot Road, Tempe, Arizona 85284, USA

⁸Laboratoire de Céramique, Ecole Polytechnique Fédérale de Lausanne, Lausanne CH 1015, Switzerland

⁹Materials Science Division, Argonne National Laboratory, Argonne, Illinois 60439, USA

Systems with a ferroelectric to paraelectric transition in the vicinity of room temperature are useful for devices. Adjusting the ferroelectric transition temperature (T_c) is traditionally accomplished by chemical substitution—as in $\text{Ba}_x\text{Sr}_{1-x}\text{TiO}_3$, the material widely investigated for microwave devices in which the dielectric constant (ϵ_r) at GHz frequencies is tuned by applying a quasi-static electric field^{1,2}. Heterogeneity associated with chemical substitution in such films, however, can broaden this phase transition by hundreds of degrees³, which is detrimental to tunability and microwave device performance. An alternative way to adjust T_c in ferroelectric films is strain^{4–8}. Here we show that epitaxial strain from a newly developed substrate can be harnessed to increase T_c by hundreds of degrees and produce room-temperature ferroelectricity in strontium titanate, a material that is not normally ferroelectric at any temperature. This strain-induced enhancement in T_c is the largest ever reported. Spatially resolved images of the local polarization state reveal a uniformity that far exceeds films tailored by chemical substitution. The high ϵ_r at room temperature in these films (nearly 7,000 at 10 GHz) and its sharp dependence on electric field are promising for device applications^{1,2}.

Enormous strains can be imparted to thin films and have previously been used to alter the T_c of ferromagnetic^{9,10} and super-

conducting^{11–13} materials. For such phenomena, strain-induced enhancements in T_c as large as tens of degrees have been observed⁹. Owing to the strong coupling between strain and ferroelectricity, much larger T_c shifts are expected^{4,6}, and have been observed^{7,8}, in ferroelectric materials.

In its pure, unstressed form, strontium titanate (SrTiO_3) is an incipient ferroelectric. It remains paraelectric down to 0 K, although chemical^{14,15} or isotopic substitution¹⁶, as well as the application of stress⁴, easily disturb this delicate state, resulting in ferroelectricity. The boundary conditions imposed by a substrate profoundly affect ferroelectricity in thin films. Figure 1 shows the predicted⁴ shift in T_c for SrTiO_3 (ref. 17) under biaxial strain $\epsilon_s = (a_{\parallel} - a_0)/a_0$, where a_0 is the lattice parameter of free-standing SrTiO_3 and a_{\parallel} is the in-plane lattice parameter of a biaxially strained (100) SrTiO_3 film. The hatched region shows the range in predicted T_c due to the spread in reported property coefficients for SrTiO_3 (refs 18, 19) that enter into the thermodynamic analysis. For example, for positive ϵ_s and $T > 120$ K, the enhancement in T_c is given by $\Delta T_c = 2\epsilon_s\epsilon_0 C(Q_{11} + Q_{12})/(s_{11} + s_{12})$, where ϵ_0 is the permittivity of free space, C is the Curie constant, Q_{11} and Q_{12} are the electrostrictive coefficients, and s_{11} and s_{12} are elastic compliances of SrTiO_3 . The breadth of the hatched region in Fig. 1 for T_c is mainly due to the nearly factor-of-two variation in the ratio of $(Q_{11} + Q_{12})/(s_{11} + s_{12})$ for what are considered the most accurate reported values of these constants. These predictions imply that a biaxial tensile strain of order 1% will shift the T_c of SrTiO_3 to the vicinity of room temperature.

In practice, the synthesis of uniformly strained ferroelectric films is challenging. Epitaxial ferroelectric films are usually grown to thicknesses greatly exceeding their critical values, resulting in undesirable relaxation towards a zero-strain state by the introduction of dislocations. Dislocation densities of $\sim 10^{11} \text{ cm}^{-2}$ are typical in epitaxial $\text{Ba}_x\text{Sr}_{1-x}\text{TiO}_3$ films²⁰, and the resulting inhomogeneous strain further smears the phase transition, in addition to the effects of chemical heterogeneity mentioned above. Our approach to controlling the properties of ferroelectric SrTiO_3 films centres on the development of new substrates that enable the growth of uniformly strained films below, or at least far closer to, the critical thickness for relaxation.

Depending on the choice of substrate, films may be grown under compressive or tensile strain. Commercially available substrates that

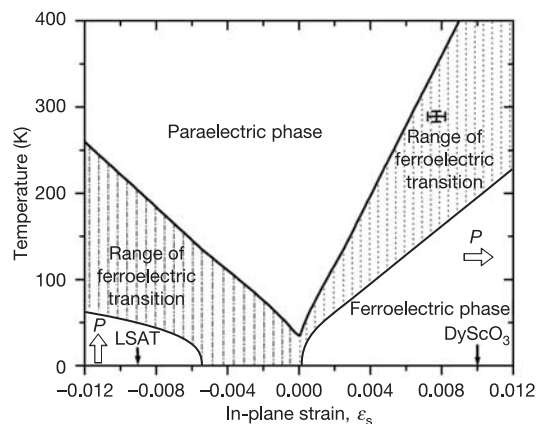


Figure 1 Expected shift in T_c of (100) SrTiO_3 with biaxial in-plane strain, based on thermodynamic analysis. The arrows indicate the predicted direction of the polarization for strained SrTiO_3 : in-plane for biaxial tensile strain and out-of-plane for biaxial compressive strain. The ϵ_s values for SrTiO_3 fully constrained (commensurate) to the lattice constants of LSAT and (110) DyScO_3 substrates are indicated by the positions of the corresponding arrows. The cross shows the observed T_c shift of a 500-Å-thick SrTiO_3 film epitaxially grown on (110) DyScO_3 .

are larger than SrTiO₃, such as KTaO₃ ($a = 3.989 \text{ \AA}$)²¹ or MgO (4.212 Å)²¹, are unsuitable for high-quality SrTiO₃ ($a = 3.905 \text{ \AA}$)¹⁸ growth because of their excessively large lattice mismatches (2.2% and 7.7%, respectively). On such substrates dislocation introduction commences soon after film nucleation, and films typically have very large mosaic spread. As the critical thickness at which dislocations begin to form varies approximately inversely with lattice mismatch, lower mismatch is desired to allow strained, low-dislocation density SrTiO₃ films to be grown that are thick enough to allow their ferroelectric properties to be conveniently probed. To produce a closer lattice match, we have developed single crystals of a new substrate material, DyScO₃, for the growth of SrTiO₃ films under uniform biaxial tensile strain. DyScO₃ is orthorhombic with lattice constants²² $a = 5.440 \text{ \AA}$, $b = 5.713 \text{ \AA}$,

and $c = 7.887 \text{ \AA}$. It is not ferroelectric down to 4 K. The (110) DyScO₃ surface has a nearly square surface mesh with an in-plane lattice spacing $a_{\parallel} = 3.944 \text{ \AA}$, resulting in a tensile lattice mismatch at room temperature (25 °C) of +1.0% with (100) SrTiO₃. For comparison, the commercial substrate (LaAlO₃)_{0.29} × (SrAl_{0.5}Ta_{0.5}O₃)_{0.71} (LSAT²³, $a = 3.869 \text{ \AA}$) with a lattice mismatch of -0.9% at room temperature was also used to grow epitaxial (100) SrTiO₃ films under uniform compressive strain. The low dielectric constants of both DyScO₃ ($\epsilon_{11} = 22.0$, $\epsilon_{22} = 18.8$ and $\epsilon_{33} = 35.5$) and LSAT ($\epsilon_r = 22.5$)²⁴ reduce field penetration in the substrate and facilitate modelling of the in-plane ϵ_r of the SrTiO₃ films when interdigitated electrodes are used²⁵, as in this study.

Reactive molecular beam epitaxy (MBE) was used to grow epitaxial SrTiO₃ films on both (110) DyScO₃ and (100) LSAT substrates. During growth the substrates were held at 650 °C and immersed in 5.0×10^{-7} torr (background pressure) of oxygen plus ~10% ozone. Reflection high-energy electron diffraction (RHEED) intensity oscillations were monitored to ensure that complete SrO and TiO₂ monolayers were deposited alternately to form the SrTiO₃ films²⁶. Although many samples were grown and characterized, the properties of a 500-Å-thick film grown on each substrate are compared below to show the effect of strain state on the ferroelectric properties of SrTiO₃.

X-ray diffraction scans show the out-of-plane lattice constant to be compressed ($a_{\perp} = 3.88 \pm 0.01 \text{ \AA}$) for the films grown on DyScO₃, and extended ($a_{\perp} = 3.93 \pm 0.01 \text{ \AA}$) for the films grown on LSAT, as expected from the boundary conditions imparted by the substrates. High-resolution X-ray diffraction measurements of the 500-Å-thick SrTiO₃ film grown on DyScO₃ reveal that its in-plane lattice constant at room temperature is $a_{\parallel} = 3.935 \pm 0.002 \text{ \AA}$, corresponding to 0.8% biaxial tensile strain. Its out-of-plane lattice constant is $a_{\perp} = 3.8785 \pm 0.0005 \text{ \AA}$. Although somewhat beyond the critical thickness at which relaxation begins to occur, the rocking curve full-width at half-maximum (FWHM) of the 200 SrTiO₃ X-ray diffraction peak is 13 arcsec (0.004°), the narrowest ever reported for an epitaxial SrTiO₃ film. This, and other aspects of the X-ray scattering measurements, indicate that this film has a higher degree of uniformity and structural perfection than is typical of Ba_xSr_{1-x}TiO₃ films. The rocking curve FWHM of the 200 SrTiO₃ peak of the 500-Å-thick SrTiO₃ film grown on LSAT was also quite narrow, 21.5 arcsec (0.006°).

Measurements of the complex dielectric permittivity were performed on the SrTiO₃ films as a function of frequency (1–20 GHz), temperature (75–330 K), and direct current (d.c.) electric field

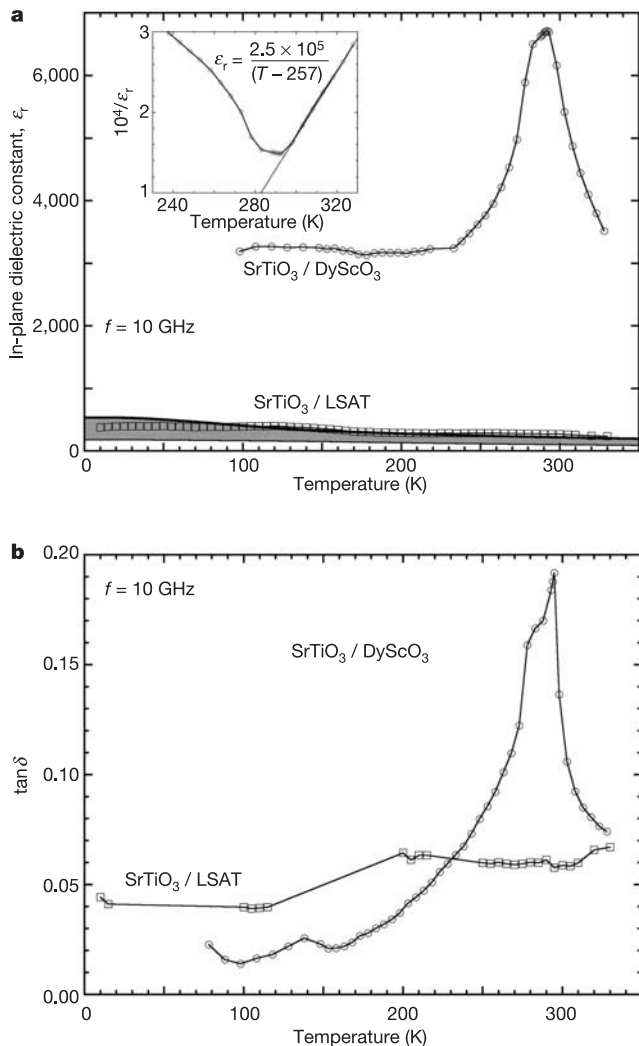


Figure 2 In-plane dielectric constant (ϵ_r) and dielectric loss ($\tan\delta$) in strained epitaxial SrTiO₃ films as a function of temperature and film thickness at a measurement frequency (f) of 10 GHz. **a, b**, Contrast of in-plane ϵ_r and $\tan\delta$, respectively, of 500-Å-thick SrTiO₃/(110) DyScO₃ and SrTiO₃/(100) LSAT epitaxial films. These films are under biaxial tensile and compressive strain, respectively. The peak in ϵ_r of about 7,000 and the simultaneous peak in $\tan\delta$ indicate that the T_c of SrTiO₃ under biaxial tension of $\epsilon_s = 0.008$ is about 293 K. The inset in **a** shows a Curie–Weiss fit to $1/\epsilon_r$. Owing to systemic errors involved in the measurement and calculation of the in-plane dielectric constant, the vertical scale in **a** may be off by as much as 10%. The shaded region in **a** corresponds to the expected value of the in-plane ϵ_r for a SrTiO₃ film commensurately strained to LSAT ($\epsilon_s = -0.009$), based on thermodynamic analysis and the range of relevant reported property coefficients for SrTiO₃ (refs 18, 19).

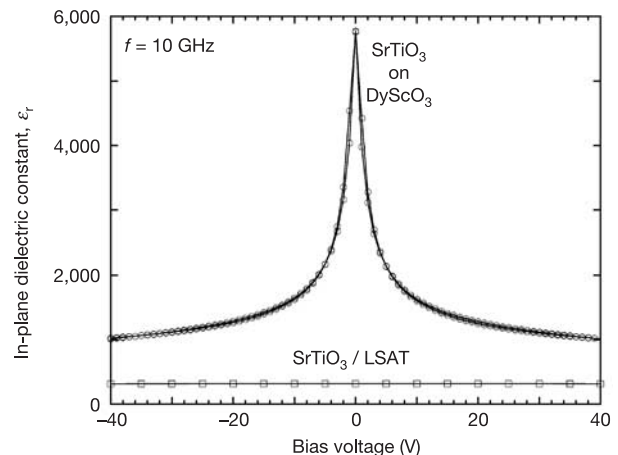


Figure 3 Dielectric tunability of the same 500-Å-thick SrTiO₃ films grown on DyScO₃ and LSAT as shown in Fig. 2. The film grown on DyScO₃ shows 82% tuning between 0 and ± 40 V at room temperature, with slight hysteresis. The film grown on LSAT exhibits ~0% tunability with the application of ± 40 V at room temperature.

(± 40 V across $6\ \mu\text{m}$) using interdigitated electrodes. The 1–2- μm -thick Ag interdigitated electrodes had 80- μm finger lengths and 6- μm finger gaps for the room-temperature measurements and 40- μm finger lengths and 12- μm finger gaps for the temperature-dependent measurements. The fingers were aligned parallel to the $\langle 110 \rangle$ in-plane directions of the SrTiO₃ films.

Figure 2 shows the temperature-dependent in-plane ϵ_r and loss tangent, $\tan\delta$, of the 500-Å SrTiO₃/DyScO₃ film measured at 10 GHz. These data are from a device acting as a microwave varactor (a voltage-tunable capacitor) with 2:1 tuning, demonstrating the technological significance of these films. The curves agree well with expected Curie–Weiss behaviour (inset) for a uniformly strained film, exhibiting a maximum in ϵ_r and $\tan\delta$ at $T_c \approx 293$ K and a Curie constant typical of displacive ferroelectrics. The peak ϵ_r of nearly 7,000 at 10 GHz is higher and the width of the peak in ϵ_r versus T is narrower than any value reported for Ba_{1-x}Sr_xTiO₃ thin films. By contrast, SrTiO₃/LSAT has a much lower dielectric constant and there is no peak in ϵ_r versus T . This result is fully consistent with the biaxial strain state causing the ferroelectric polarization to lie in the plane of the film for SrTiO₃ on DyScO₃, the direction sensed by the interdigitated electrodes, but lying out-of-plane of the SrTiO₃ grown on LSAT.

The observed T_c shift surpasses all prior records^{7,8} and gives credence to prior work on SrTiO₃/SrZrO₃ superlattices where ferroelectricity at room temperature in 8-nm-thick strained SrTiO₃ layers was assumed to be responsible for the dielectric properties of the composite superlattice²⁷. Our results are consistent with a strain-induced phenomenon; the possibility that minute Sc doping from the DyScO₃ substrate is in part responsible for the dramatic changes in dielectric behaviour is also being investigated, although no such effects have ever been reported²⁸.

The remarkable field sensitivity of ϵ_r , which drops by 82% for an

applied voltage of 40 V across 6 μm gaps, is shown in Fig. 3. Such large tuning with modest fields makes these films applicable to a variety of microwave applications. As is typical of ferroelectric thin films, their properties depend on thickness (Supplementary Information).

Optical measurements of the ferroelectric polarization at microwave driving fields were performed using time-resolved confocal scanning optical microscopy (TRCSOM)^{29,30}. The in-phase and out-of-phase response at the microwave driving frequency correspond to the real and imaginary parts of the polar contribution to the dielectric response at that frequency.

Figure 4c shows a typical TRCSOM image of the phase shift between linear electro-optic response and a microwave driving field (3.27 GHz), measured for the 500 Å SrTiO₃/DyScO₃ film. The electro-optic phase is computed from a fit to the temporal response at various points in the microwave drive cycle^{29,30}. Most striking are the large regions in which the phase is essentially uniform, separated by sharp boundaries at which the phase changes by 90° or 180°. These boundaries correspond to features observed by atomic force microscopy (AFM) on the film (Fig. 4a) as well as on bare DyScO₃ substrates, and may be due to surface imperfections that break the in-plane symmetry and produce an easy axis for the SrTiO₃ films. For sake of comparison, Fig. 4d shows a typical TRCSOM image (at a fixed time delay) for a ferroelectric film (Ba_{0.5}Sr_{0.5}TiO₃/MgO) that has not been strain-engineered. The strong fluctuations in the electro-optic response on submicrometre scales are typical of films that are inhomogeneously strained.

The remarkable dielectric properties of SrTiO₃, while recognized for many decades, have previously only been accessible in the bulk and at cryogenic temperatures. Efforts to shape the properties of ferroelectric films have been restricted by available substrates. Through controlled substrate engineering, often overlooked in the growth of thin films, we have achieved ϵ_r and tunability at room temperature in SrTiO₃ films with properties comparable to bulk SrTiO₃ at cryogenic temperatures. In addition to radically enhanced dielectric properties, we expect other ferroelectric properties (including pyroelectric, piezoelectric and nonlinear optical) of SrTiO₃ to be accessible at room temperature through the application of appropriate homogeneous strain. □

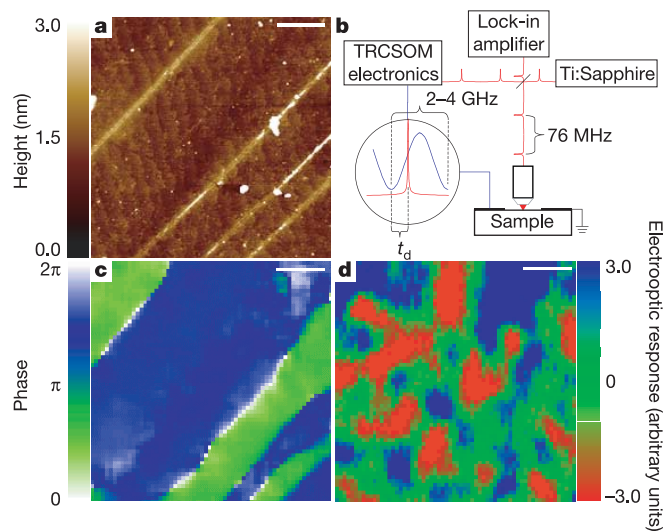


Figure 4 Comparison of the morphology and microwave electro-optic response of tunable dielectric films at room temperature (just above T_c). The scale bars are $1\ \mu\text{m}$ for all images. **a**, An AFM image of the same 500-Å-thick SrTiO₃ film grown on DyScO₃ shown in Fig. 2. In addition to unit-cell-high steps on the surface of the SrTiO₃ film, four diagonal linear features that protrude ~ 50 Å from the surface are evident. Similar surface imperfections are seen on the bare substrates, suggesting that they are associated with polishing. **b**, Schematic of the TRCSOM technique used for imaging ferroelectric polarization at microwave frequencies. **c**, Images of the phase shift between the electro-optic response and microwave driving field (3.27 GHz) for the same SrTiO₃/DyScO₃ film (but not the identical region) as in **a**, revealing uniform in-plane polarization separated by clear boundaries like the ones observed by AFM. **d**, TRCSOM image (at one time delay) of a typical epitaxial Ba_{0.5}Sr_{0.5}TiO₃/MgO film at 2.06 GHz, showing inhomogeneous in-plane polarization.

Received 12 March; accepted 22 June 2004; doi:10.1038/nature02773.

- Vendik, O. G. *Ferroelectrics for Microwave Applications* (Soviet Radio, Moscow, 1979).
- Lancaster, M. J., Powell, J. & Porch, A. Thin-film ferroelectric microwave devices. *Supercond. Sci. Technol.* **11**, 1323–1334 (1998).
- Hubert, C. *et al.* Confocal scanning optical microscopy of Ba_{0.5}Sr_{0.5}TiO₃ thin films. *Appl. Phys. Lett.* **71**, 3353–3355 (1997).
- Devonshire, A. F. Theory of ferroelectrics. *Phil. Mag Suppl.* **3**, 85–130 (1954).
- Uwe, H. & Sakudo, T. Stress-induced ferroelectricity and soft phonon modes in SrTiO₃. *Phys. Rev. B* **13**, 271–286 (1976).
- Pertsev, N. A., Zembilgotov, A. G. & Tagantsev, A. K. Effect of mechanical boundary conditions on phase diagrams of epitaxial ferroelectric thin films. *Phys. Rev. Lett.* **80**, 1988–1991 (1998).
- Abe, K. *et al.* Modification of ferroelectricity in heteroepitaxial (Ba,Sr)TiO₃ films for non-volatile memory applications. *Integr. Ferroelectr.* **21**, 197–206 (1998).
- Streiffer, S. K. *et al.* Observation of nanoscale 180° stripe domains in ferroelectric PbTiO₃ thin films. *Phys. Rev. Lett.* **89**, 067601 (2002).
- Beach, R. S. *et al.* Enhanced Curie temperatures and magnetoelastic domains in Dy/Lu superlattices and films. *Phys. Rev. Lett.* **70**, 3502–3505 (1993).
- Gan, Q., Rao, R. A., Eom, C. B., Garrett, J. L. & Lee, M. Direct measurement of strain effects on magnetic and electrical properties of epitaxial SrRuO₃ thin films. *Appl. Phys. Lett.* **72**, 978–980 (1998).
- Lock, J. M. Penetration of magnetic fields into superconductors. III. Measurements on thin films of tin, lead and indium. *Proc. R. Soc. Lond. A* **208**, 391–408 (1951).
- Sato, H. & Naito, M. Increase in the superconducting transition temperature by anisotropic strain effect in (001) La_{1.85}Sr_{0.15}CuO₄ thin films on LaSrAlO₄ substrates. *Physica C* **274**, 221–226 (1997).
- Bozovic, I., Logvenov, G., Belca, I., Narimbetov, B. & Svetlo, I. Epitaxial strain and superconductivity in La_{2-x}Sr_xCuO₄ thin films. *Phys. Rev. Lett.* **89**, 107001 (2002).
- Bednorz, J. G. & Müller, K. A. Sr_{1-x}Ca_xTiO₃: An XY quantum ferroelectric with transition to randomness. *Phys. Rev. Lett.* **52**, 2289–2292 (1984).
- Ang, C. *et al.* Dielectric polarization processes in Bi:SrTiO₃. *J. Phys. Chem. Solids* **61**, 191–196 (2000).
- Itoh, M. *et al.* Ferroelectricity induced by oxygen isotope exchange in strontium titanate perovskite. *Phys. Rev. Lett.* **82**, 3540–3543 (1999).
- Pertsev, N. A., Tagantsev, A. K. & Setter, N. Phase transitions and strain-induced ferroelectricity in SrTiO₃ epitaxial thin films. *Phys. Rev. B* **61**, R825–R829 (2000).
- Hellwege, K.-H. & Hellwege, A. M. (eds) *Landolt-Börnstein: Numerical Data and Functional Relationships in Science and Technology* New Series, Group III, Vol. 16a, 59–64 (Springer, Berlin, 1981).

19. Hellwege, K.-H. & Hellwege, A. M. (eds) *Landolt-Börnstein: Numerical Data and Functional Relationships in Science and Technology* New Series, Group III, Vol. 11, 418 (Springer, Berlin, 1979).

20. Canedy, C. L. *et al.* Dielectric properties in heteroepitaxial Ba_{0.6}Sr_{0.4}TiO₃ thin films: Effect of internal stresses and dislocation-type defects. *Appl. Phys. Lett.* **77**, 1695–1697 (2000).

21. Hellwege, K.-H. & Hellwege, A. M. (eds) *Landolt-Börnstein: Numerical Data and Functional Relationships in Science and Technology* New Series, Group III, Vol. 7b, 26; Vol. 7e, 635 (Springer, Berlin, 1976).

22. JCPDS Powder Diffraction File: Sets 27 to 28 72 (Card 27–204, JCPDS International Centre for Diffraction Data, Swarthmore, 1986).

23. Chakoumakos, B. C., Schlom, D. G., Urbanik, M. & Luine, J. Thermal expansion of LaAlO₃ and (La,Sr)(Al,Ta)O₃, substrate materials for superconducting thin-film device applications. *J. Appl. Phys.* **83**, 1979–1982 (1998).

24. Tidrow, S. C. *et al.* New substrates for HTSC microwave devices. *IEEE Trans. Appl. Supercond.* **7**, 1766–1768 (1997).

25. Gevorgian, S. S., Martinsson, T., Linnér, P. L. J. & Kollberg, E. L. CAD models for multilayered substrate interdigital capacitors. *IEEE Trans. Microwave Theory Tech.* **44**, 896–904 (1996).

26. Haeni, J. H., Theis, C. D. & Schlom, D. G. RHEED intensity oscillations for the stoichiometric growth of SrTiO₃ thin films by reactive molecular beam epitaxy. *J. Electroceram.* **4**, 385–391 (2000).

27. Christen, H.-M., Knauss, L. A. & Harshvardhan, K. S. Field-dependent dielectric permittivity of paraelectric superlattice structures. *Mater. Sci. Eng. B* **56**, 200–203 (1998).

28. Lemanov, V. V., Sotnikov, A. V., Smirnova, E. P. & Weihnacht, M. Giant dielectric relaxation in SrTiO₃–SrMg_{1/3}Nb_{2/3}O₃ and SrTiO₃–SrSc_{1/2}Ta_{1/2}O₃ solid solutions. *Fiz. Tverd. Tela (St Petersburg)* **44**, 1948–1957 (2002).

29. Hubert, C. & Levy, J. New optical probe of GHz polarization dynamics in ferroelectric thin films. *Rev. Sci. Instrum.* **70**, 3684–3687 (1999).

30. Hubert, C., Levy, J., Cukauskas, E. J. & Kirchoefer, S. W. Mesoscopic microwave dispersion in ferroelectric thin films. *Phys. Rev. Lett.* **85**, 1998–2001 (2000).

Supplementary Information accompanies the paper on www.nature.com/nature.

Acknowledgements We acknowledge discussions and interactions with M. D. Biegalski, J. Schubert, S. Trolier-McKinstry and J. Mannhart during the course of this work. In addition, the financial support of the National Science Foundation, the Office of Naval Research for the work performed at NRL, the Swiss National Science Foundation, and, for the work performed at ANL, the US Department of Energy, Basic Energy Sciences—Materials Sciences is gratefully acknowledged.

Competing interests statement The authors declare that they have no competing financial interests.

Correspondence and requests for materials should be addressed to D.G.S. (schlom@ems.psu.edu).

Bulk glasses and ultrahard nanoceramics based on alumina and rare-earth oxides

A. Rosenflanz, M. Frey, B. Endres, T. Anderson, E. Richards & C. Schardt

3M Central Research Laboratory, Corporate Research & Development, 3M Company, St Paul, Minnesota 55144-1000, USA

Although often regarded as a network-former in conventional silicate glasses, Al₂O₃ alone cannot be obtained as a bulk glass. Until now, glasses comprising continuously linked [AlO_x] polyhedra have been prepared in only a few systems under very fast cooling conditions, which limits their dimensions to a few millimetres^{1–3}. Yet it is desirable to prepare bulk, or monolithic, alumina-rich glasses, with the prospect of superior mechanical, chemical and optical properties⁴. Here we report a novel process for preparing very-high-alumina glasses and nanoscale glass-ceramics. Fully dense bulk articles in net shape are obtained through viscous sintering of glass microbeads. Additional heat treatment of the consolidated glasses leads to fully crystallized transparent glass-converted nanoceramics with a hardness similar to that of alumina. This method avoids the impracticably high applied pressures (more than 1 GPa) that have been required in most cases to prepare nanocrystalline ceramics by sintering, owing to the concurrent nature of densification and grain growth under pressureless conditions^{5,6}. The reported techniques can be

extended to form glasses and nanoceramics in other oxide systems that do not include a conventional glass-forming component.

Elemental and oxide melts lacking conventional glass-formers such as sulphur or silica are prone to crystallization during slow cooling. To form glasses they must be ‘kinetically frozen’ by rapid quenching, as originally shown for metals⁷. Typically, slower cooling rates can be used for multicomponent eutectic compositions in which ratios of glass transition temperatures T_g relative to the melting point T_m are higher^{8,9}. For example, Al₂O₃, a reluctant glass former, necessitates quenching rates as high as 10⁷ K s⁻¹ to retain an amorphous state^{10,11}. However, when alloyed in eutectic proportions with other oxides, notably CaO or RE₂O₃ (where RE stands for rare earth), glasses can be generated at cooling rates of less than 10³ K s⁻¹ (refs 3, 12, 13). These rates are nevertheless still too high to obtain bulk (more than 1 cm) glasses, limiting the achievable forms to thin films, ribbons, fibres and small spheres.

Sintering of conventional glass frit into coherent, dense, bulk forms is a well-known method in which free surfaces are eliminated by viscous flow at temperatures above T_g . For glasses that do not devitrify, there is little restriction on the sintering temperatures. However, many quenched glasses crystallize rapidly at temperatures T_x when the supplied thermal energy mobilizes the structure and the latent heat previously trapped during quenching is released. The working temperature of such glasses is thus restricted to between T_g and T_x . The successful exploitation of this kinetic window, $\Delta T_x = T_x - T_g$, was instrumental in the development of bulk metallic glasses from glassy powders a decade ago¹⁴, but it had not been applied to non-silicate oxides. However, thermal analysis data indicate that a sizable window of ΔT_x exists in a rare-earth–alumina system, and ‘jelly-like’ formability of Al₂O₃–Gd₂O₃ glass fibres, when heated inside the ΔT_x regime, has been reported¹⁵. Here we show that the compositional control of this kinetic window provides an easy path to the preparation of bulk glasses and nanocrystalline glass-ceramics in a variety of non-conventional glass-forming oxide systems.

Alumina–rare-earth oxide systems (Al₂O₃–RE₂O₃) were chosen for this study because of their technological importance. Binary

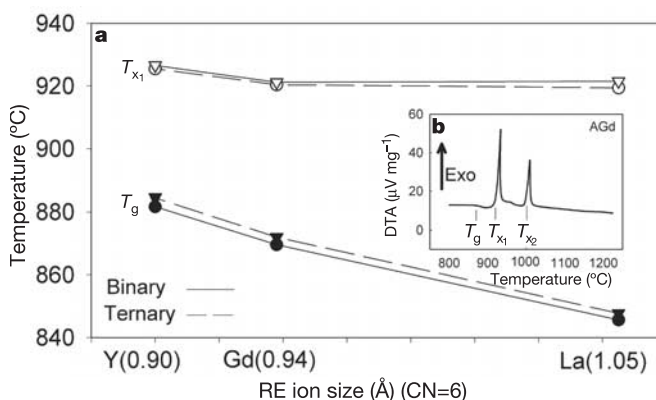


Figure 1 Effect of rare-earth ion size on ΔT_x . **a**, Glass transition (T_g) and crystallization (T_x) temperatures of binary (solid lines) and ternary (dashed lines) glasses as a function of the ionic radius of the rare-earth (RE) cation. CN, coordination number. **b**, DTA trace of 77 Al₂O₃–23 Gd₂O₃ (mol. %) glass heated at 10 °C min⁻¹. Although two exothermic events— T_{x1} and T_{x2} —were frequently observed in these glasses, only the first (T_{x1}) reflects the crystallization event, whereas T_{x2} is thought to be caused by a liquid–liquid transition from a metastable high-density amorphous phase to more stable low-density amorphous phase²⁷. In ternary liquids, the T_{x2} peak was essentially absent, which might have been caused by higher viscosities of these liquids and the retention of a single (high-density amorphous) phase during cooling. Throughout the article, T_x is identified with T_{x1} .